# Quasiparticle dynamics in reshaped helical Dirac cone of topological insulators

Lin Miao[a,1], Z. F. Wang[b,1], Wenmei Ming[b], Meng-Yu Yao[a], Meixiao Wang[a], Fang Yang[a], Y. R. Song[a], Fengfeng Zhu[a], Alexei V. Fedorov[c], Z. Sun[d], C. L. Gao[a], Canhua Liu[a], Qi-Kun Xue[e], Chao-Xing Liu[f], Feng Liu[b,2], Dong Qian[a,2], and Jin-Feng Jia[a,2]

[a]Department of Physics, Key Laboratory of Artificial Structures and Quantum Control (Ministry of Education), Shanghai Jiao Tong University, Shanghai 200240, China; [b]Department of Materials Science and Engineering, University of Utah, Salt Lake City, UT 84112; [c]Advanced Light Source, Lawrence Berkeley National Laboratory, Berkeley, CA 94720; [d]National Synchrotron Radiation Laboratory, University of Science and Technology of China, Hefei 230026, China; [e]Department of Physics, State Key Laboratory for Low-Dimensional Quantum Physics, Tsinghua University, Beijing 100084, China; and [f]Department of Physics, The Pennsylvania State University, University Park, PA 16802

Edited by Allan H. MacDonald, University of Texas at Austin, Austin, TX, and approved January 4, 2013 (received for review October 17, 2012)

**Topological insulators and graphene present two unique classes of materials, which are characterized by spin-polarized (helical) and nonpolarized Dirac cone band structures, respectively. The importance of many-body interactions that renormalize the linear bands near Dirac point in graphene has been well recognized and attracted much recent attention. However, renormalization of the helical Dirac point has not been observed in topological insulators. Here, we report the experimental observation of the renormalized quasiparticle spectrum with a skewed Dirac cone in a single Bi bilayer grown on $Bi_2Te_3$ substrate from angle-resolved photoemission spectroscopy. First-principles band calculations indicate that the quasiparticle spectra are likely associated with the hybridization between the extrinsic substrate-induced Dirac states of Bi bilayer and the intrinsic surface Dirac states of $Bi_2Te_3$ film at close energy proximity. Without such hybridization, only single-particle Dirac spectra are observed in a single Bi bilayer grown on $Bi_2Se_3$, where the extrinsic Dirac states Bi bilayer and the intrinsic Dirac states of $Bi_2Se_3$ are well separated in energy. The possible origins of many-body interactions are discussed. Our findings provide a means to manipulate topological surface states.**

Dirac fermion | electronic structures | thin films

Much recent attention has been devoted to graphene (1–6) and topological insulators (TIs) (7–18), two unique material systems that exhibit conical linear electron bands of Dirac spectra. quasiparticles of Dirac fermions are distinct from those of ordinary Fermi liquids (19–21). Although rather difficult and rare, recent angle-resolved photoemission spectroscopy (ARPES) experiments (1, 2, 5, 6) have directly shown the existence of many-body quasiparticle spectra near Dirac point in graphene, manifesting electron–electron, electron–phonon, and electron–plasmon interactions. Similar to graphene, TIs also possess Dirac cone, albeit it is spin-polarized or helical Dirac cone. So far, however, no renormalized quasiparticle spectra near the helical Dirac point similar to graphene have been reported in any known TIs, and most studies of TIs are based on the single-particle picture (9, 11, 12, 14, 18). Here, we report direct experimental observation of a skewed helical Dirac point, a signature quasiparticle spectrum indicative of many-body interactions, by ARPES in a TI system of Bi(111) bilayer grown on $Bi_2Te_3$ substrate, where a 2D TI is interfaced with a 3D TI (22).

ARPES can probe the quasiparticle's scattering rate at different energy scales, and therefore can access the many-body interactions directly (23). Our experimental observation of the quasiparticle spectra manifesting many-body effects is characterized with a "vertically nondispersive" feature near Dirac point. Based on model density functional theory (DFT) calculations of electron bands as a function of the artificially changed interfacial distance between the Bi bilayer and substrate, we found that the renormalized quasiparticle spectra in $Bi/Bi_2Te_3$ are likely associated with the strong hybridization between the substrate-induced Dirac states of Bi bilayer and the surface Dirac states of $Bi_2Te_3$ substrate at close energy proximity. When these two Dirac states are well separated in energy without the hybridization, such as in $Bi/Bi_2Se_3$, only single-particle Dirac spectra are observed without the feature of many-body interactions. We further discuss possible physical origins of the observed many-body spectra, and we are able to exclude the electron–phonon interaction.

## Results and Discussion

We have grown Bi(111) films in the layer-by-layer mode on the (111)-oriented $Bi_2Te_3$ and $Bi_2Se_3$ substrates. The growth mode is studied by reflection high-energy electron diffraction (RHEED) and scanning tunneling microscopy (STM) (details can be found in the *Supporting Information*). The in-plane lattice constant is measured to match the substrate exactly with a perfect coherent interface, so that the Bi(111) film is under 3.5% and 9.0% tensile strain on $Bi_2Te_3$ or $Bi_2Se_3$, respectively. Here, we focus on electronic properties of single Bi(111) bilayer grown on both substrates by measuring the electron band structures using ARPES.

The band structures of the bare $Bi_2Te_3$ and $Bi_2Se_3$ substrates near the Fermi level around zone center (Γ-point) are presented in Fig. 1 *A* and *F*, respectively. Linearly dispersive energy bands from surface states forming a Dirac cone at the Γ-point (14) are well separated from bulk bands. Known from previous ARPES studies and first-principles calculations (13, 14), the Dirac point of $Bi_2Te_3$ is hidden by the "M"-shaped bulk valence bands. In our films, the hidden Dirac point can be located at ∼0.2 eV below Fermi level by extrapolating the "V"-shaped surface bands. Similar to previous study (12), the Dirac point of $Bi_2Se_3$ is inside the bulk gap, located at ∼0.3 eV below Fermi level.

The electronic band structures are observed to change dramatically when a single Bi(111) bilayer is grown. On $Bi_2Te_3$, the M-shaped bulk bands disappear, as seen in Fig. 1 *B* and *C*. Most surprisingly, we see two sets of linearly dispersive bands crossing at Γ-point, one at the energy slightly above 0.2 eV and the other slightly below 0.2 eV, which is the location of the hidden Dirac point of bare $Bi_2Te_3$ film (Fig. 1*A*). In a recent study, it was thought there was only one Dirac point in this energy range (22) due to the limited ARPES momentum resolution. With substantial improvement of film quality and ARPES resolution, two Dirac crossing

Author contributions: C.L.G., D.Q., and J.-F.J. designed research; L.M., Z.F.W., W.M., M.-Y.Y., M.W., F.Y., Y.R.S., F.Z., A.V.F., Z.S., F.L., and D.Q. performed research; L.M., Z.F.W., W.M., C.L., C.-X.L., Q.-K.X., F.L., D.Q., and J.-F.J. analyzed data; and Z.F.W., F.L., and D.Q. wrote the paper.

The authors declare no conflict of interest.

This article is a PNAS Direct Submission.

[1]L.M. and Z.F.W. contributed equally to this work.

[2]To whom correspondence may be addressed. E-mail: dqian@sjtu.edu.cn, fliu@eng.utah.edu, or jfjia@sjtu.edu.cn.

This article contains supporting information online at www.pnas.org/lookup/suppl/doi:10.1073/pnas.1218104110/-/DCSupplemental.

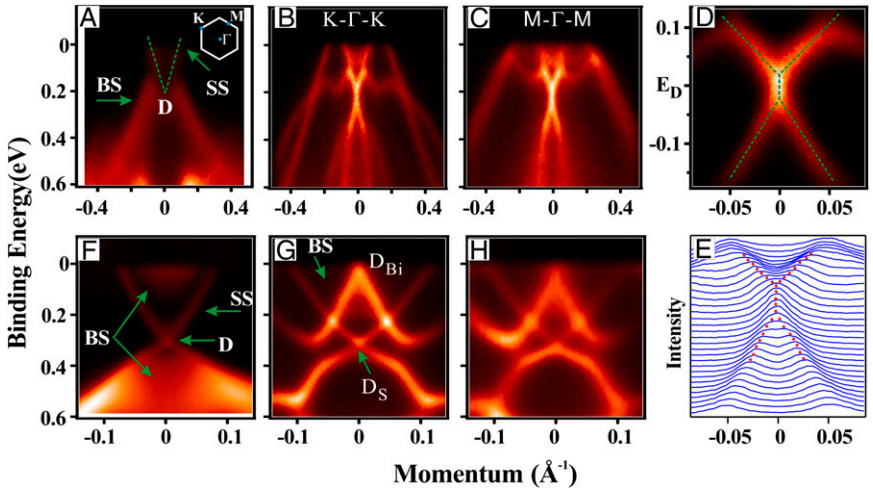


**Fig. 1.** Experimental band dispersions along high-symmetry directions. (*A*) ARPES spectra of 40 QLs $Bi_2Te_3$ film along K–Γ–K cut. Green lines mark the linearly dispersive V-shaped surface bands. The Dirac point D at the binding energy of ∼0.2 eV is hidden by the M-shaped BS valence bands. The Fermi level lies in the bulk energy gap. No bulk conduction bands were observed. (*Inset*) First surface Brillouin zone of the system. K and M are the high-symmetric points. BS, bulk state. (*B*) ARPES spectra of one bilayer Bi(111) film on $Bi_2Te_3$ along K–Γ–K and (*C*) along M–Γ–M. The V- and Λ–shaped bands split vertically away from the original Dirac point D of bare $Bi_2Te_3$ film. The M-shaped BS bands disappear. (*D*) High-resolution ARPES spectra showing the two split upper-V and lower-Λ bands, as marked by green lines and (*E*) corresponding MDCs showing the nondispersive feature between the V and Λ bands. Red dots mark the band dispersions from MDC fitting. (*F*) ARPES spectra of bare $Bi_2Se_3$. A sharp Dirac point is seen at ∼0.3 eV below Fermi level. Due to intrinsic n-doping, bulk conduction bands were observed surrounded by SS bands. SS, surface state. (*G*) ARPES spectra of one bilayer Bi(111) on $Bi_2Se_3$ along K–Γ–K and (*H*) along M–Γ–M. Two Dirac points are seen as marked, $D_S$ and $D_{Bi}$.

points are clearly resolved, with a magnified view shown in Fig. 1*D*. The upper "V" and lower "Λ" Dirac cone do not touch, and most interestingly, there appears a vertically nondispersive feature between them with an energy width of ∼0.05 eV. This can also be clearly seen in the momentum distribution curves (MDCs), as shown in Fig. 1*E*. In this "vertical" region, MDCs only have a single peak. The Fermi velocity ($v_F$) of the V and Λ bands is $\sim 3.2 \times 10^5$ m/s and $\sim 4.5 \times 10^5$ m/s, respectively. The $v_F$ of the V band in the bare $Bi_2Te_3$ film (Fig. 1*A*) is $\sim 4.5 \times 10^5$ m/s. Electrons between V and Λ bands would have infinite velocity if the measured signals were real single-particle spectra. We do not believe that is the case.

The renormalization of linearly dispersive Dirac cone is a well-known signature of quasiparticle spectrum arising from many-body interactions (1–6). We found that such quasiparticle TI spectrum is unique to the $Bi/Bi_2Te_3$ system. Even in a similar and closely related $Bi/Bi_2Se_3$ system, only ordinary single-particle TI spectra are observed, as shown in Fig. 1 *G* and *H*. Two well-separated Dirac points at different energies (marked as $D_S$ and $D_{Bi}$) are seen in Fig. 1 *H* and *G*. $D_S$ is located at ∼0.3 eV below Fermi level, almost at the same position as the Dirac point in the bare $Bi_2Se_3$ (Fig. 1*F*). $v_F$ near $D_S$ is $\sim 2.8 \times 10^5$m/s, which is about half of $v_F$ in bare $Bi_2Se_3$ film ($5.7 \times 10^5$ m/s, Fig. 1*F*). $D_{Bi}$ is very close to Fermi level with a $v_F \sim 5.3 \times 10^5$ m/s. Most noticeably, no vertically nondispersive feature is visible in either $D_S$ or $D_{Bi}$.

The 2D character of the observed linearly dispersive bands is further confirmed by the photon-energy–dependent experiments that are widely used to separate surfaces states from bulk bands (11). By tuning incident photon energy, we change the detectable momentum along the film's normal direction ($k_z$). Consequently, the measured energy band dispersions from bulk contributions will change as a function of incident photon energy. Fig. 2 shows the ARPES spectra under different incident photon energies (more spectra can be found in the *Supporting Information*). Except for the relative spectral weight or intensity, the band dispersions and the location of Dirac cone do not change. This indicates that the observed energy bands are coming only from 2D Bi bilayer and/or surface states of TI substrates.

The observation of quasiparticle TI spectrum and the fact that it only occurs in $Bi/Bi_2Te_3$ but not in $Bi/Bi_2Se_3$ are both very intriguing. To help understand the physical origin of the quasiparticle TI spectrum in $Bi/Bi_2Te_3$ and the underlying difference between these two systems, we have performed DFT calculations of electron band structures of both systems. Fig. 3 *A–D* shows the

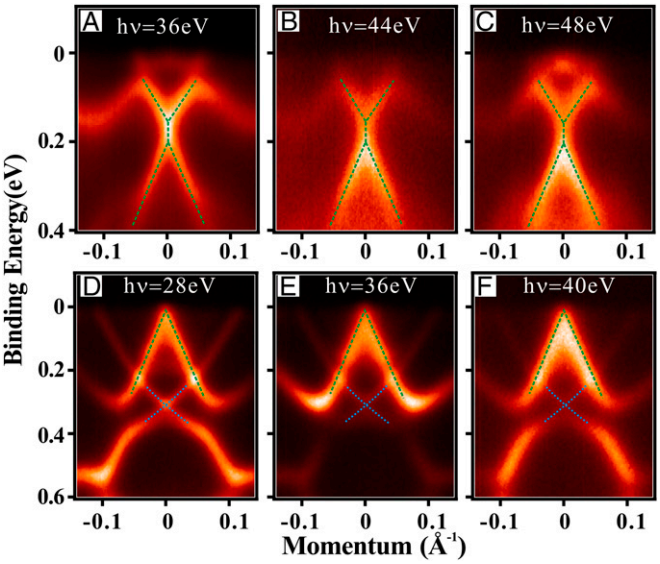


**Fig. 2.** Photon energy dependence of the ARPES spectra. (*A–C*) Bi/ $Bi_2Te_3$. Green lines mark the linearly dispersive bands and the nondispersive feature. (*D–F*) $Bi/Bi_2Se_3$. Blue lines mark the Dirac cone from $Bi_2Se_3$; green lines mark the new Dirac cone from Bi bilayer. By changing incident photon energy, the $k_z$ of the detected energy bands changes. The observed dispersion relations of all of the linearly dispersive bands do not change at all, which indicates their 2D characters. Relative intensity of the bands changes under different photon energy because of the photoemission matrix element effects and/or changing electron escape length.

PHYSICS

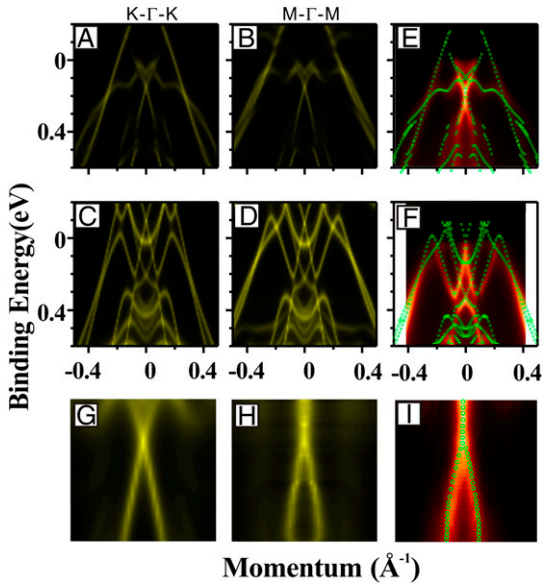


**Fig. 3.** Theoretical energy bands and self-energy correction. (*A* and *B*) Bi/$Bi_2Te_3$ (only contributions from top Bi bilayer are plotted). (*C* and *D*) Bi/$Bi_2Se_3$ (contributions from top Bi bilayer plus upper 2 QL $Bi_2Se_3$ are plotted). (*E*) Experimental bands of Bi/$Bi_2Te_3$ along K–Γ–K cut superimposed with theoretical bands (green open circles). (*F*) Experimental bands of Bi/$Bi_2Se_3$ along M–Γ–M superimposed with theoretical bands (green open circles). The Fermi levels are shifted to the same position. (*G* and *H*) Magnified theoretically calculated Dirac cones (*G*) without and (*H*) with self-energy correction for Bi/$Bi_2Te_3$. (*I*) The experimental quasiparticle spectrum superimposed with theoretical spectrum extracted from *H* (green open circles) to illustrate the nondispersive feature near Dirac point. Note that the DFT bands (*A–D*, *G*, and *H*) are broadened by a Lorentzian width of ∼20 meV to better show the spectral functions, but they are not to be confused with self-energy correction (*H*), because they will only uniformly broaden the width of all of the bands but not the relative width nor the position of the bands, as the self-energy correction will do.

calculated bands of Bi/$Bi_2Te_3$ and Bi/$Bi_2Se_3$ systems along high-symmetry directions. In both systems, the Dirac cone structures are all helical Dirac cones *Supporting Information*). Fig. 3 *E* and *F* shows the experimental bands overlaid with the calculated bands. We see that overall the agreement of band energies and dispersions between experiment and calculation is very good except for the slightly shifted Fermi level. However, there is one significant discrepancy in Fig. 3*E*: The experiment shows a nondispersive feature between two vertically separated V and Λ Dirac cones as discussed above, whereas the calculation shows two Dirac cones crossing at one point as for a typical single-particle Dirac-cone spectrum. This indicates that the observed nondispersive feature is originated from many-body interactions that cannot be reproduced by DFT calculations of single-particle spectrum.

To further support the above point, we have extracted the self-energies from the experimental data and incorporated them into the calculated single-particle spectral functions (see the magnified view near Γ-point in Fig. 3*G*) to construct the quasiparticle spectra (details can be found in *Supporting Information*). Fig. 3*H* shows the resulting quasiparticle spectral function with the self-energy correction near Γ-point. The single-point–crossing Dirac cone (Fig. 3*G*) elongates vertically into a nondispersive feature between two Dirac V and Λ points (Fig. 3*H*), in good agreement with the experimental spectra, as shown in Fig. 3*I*, where the experimental bands are overlaid with the theoretical bands. Here, the purpose of our theoretical fitting is mainly to show the qualitative importance of the self-energy correction, but the extracted self-energies should be treated with caution. This is because accurate quantitative values will need to be extracted from much more extended higher-resolution ARPES data. On the other hand, as seen from Fig. 3 *C* and *D*, there are two Dirac cones in the Bi/$Bi_2Se_3$ system.

We further performed spectral analysis to better understand the DFT band structures. The projected spectral function calculations show that the calculated Dirac cone at ∼0.15 eV below Fermi level (Fig. 3 *A* and *B*) is a hybrid Dirac state between the Bi bilayer and the bulk $Bi_2Te_3$ film, with ∼50% spectral weight coming from the Bi bilayer. This is very surprising, considering that the single Bi (111) bilayer is well-known to have a finite gap (24–27). It turns out to be caused by a hybridization of two Dirac states, one intrinsic from $Bi_2Te_3$ substrate and the other extrinsic from Bi bilayer induced by the interface (see *Discussion* below). A recent study had assigned this Dirac cone to $Bi_2Te_3$ without knowing about the second Bi Dirac cone, although they did see the charge density of this Dirac state leaked into Bi (22). In the Bi/$Bi_2Se_3$ system, 90% of its spectral weight of the Dirac cone at ∼0.1 eV above the Fermi level (Fig. 3 *C* and *B*) comes from the Bi bilayer with little hybridization with the substrate states. The second Dirac cone at ∼0.2 eV below the Fermi level fully comes from $Bi_2Se_3$.

If one looks at the calculated band structure of Bi/$Bi_2Te_3$ (Fig. 3 *A* and *B*) alone, there appears to be only one Dirac point, presumably coming from the $Bi_2Te_3$ substrate. In contrast, the calculated band structure of Bi/ $Bi_2Se_3$ (Fig. 3 *C* and *D*) clearly shows two Dirac points. To resolve this difference, we have performed a set of "model" calculations by artificially increasing the interfacial distance between the Bi bilayer and $Bi_2Te_3$ (or $Bi_2Se_3$) substrate to gradually tune the interface coupling strength, as shown in Figs. 4 and 5. These systematic model calculations reveal that both systems have a second Dirac point produced by the Bi bilayer due to interfacial interaction. Interestingly, it just happens that at the equilibrium distance, the interface-induced Bi Dirac point lies at almost the same energy as the $Bi_2Te_3$ Dirac point, so it appears as if there was only one Dirac point in Fig. 4*E*, as we discuss below.

The bands in Fig. 4*D* at large interface separation represent essentially the strained freestanding Bi bilayer bands at the $Bi_2Te_3$ lattice constant. Projecting the spectral functions onto the top Bi bilayer with the decreasing interfacial distance (from Fig. 4 *D* to Fig. 4*A*), we found that the interaction between the Bi and substrate gradually splits the degenerated Bi bands (Fig. 4*D*), and the Dirac cone ($D_h$ in Fig. 4*A*) partially comes from the lower branch of the Bi band. We also projected the spectral functions onto the top Bi bilayer plus upper two quintuple layers (QL) $Bi_2Te_3$ (Fig. 4 *E–H*), to see what happens to the "bulk" Dirac cone ($D_S$) of $Bi_2Te_3$ film in this process. In Fig. 4*H* (4 Å away from the equilibrium distance), we can clearly see the bulk Dirac cone. However, with the decreasing interfacial distance (from Fig. 4*H* to Fig. 4*E*), the interaction blurs the bulk Dirac cone (Fig. 4*H*), making it indistinguishable from the substrate-induced Bi bilayer Dirac cone at the equilibrium distance (Fig. 4*E*), and the two hybridize into the $D_h$.

For comparison, the Bi/$Bi_2Se_3$ results are shown in Fig. 5. The bands in Fig. 5*D* at large interface separation represent essentially the strained freestanding Bi bilayer bands at the $Bi_2Se_3$ lattice constant, which is to be noted as different from Fig. 4*D*. Similar to the Bi/$Bi_2Te_3$ system, there is also a substrate-induced Dirac cone ($D_{Bi}$) forming from the lower branch of the Bi bilayer band, but different from the Bi/$Bi_2Te_3$ system, its position is about ∼0.1 eV above the Fermi level (Fig. 5*A*) and about 90% of its spectral weight comes from the Bi bilayer having little hybridization with the substrate states. Changing the interfacial distance, the position of the bulk $Bi_2Se_3$ Dirac cone ($D_S$) is almost unchanged, staying at ∼0.2 eV below the Fermi level, as shown in Fig. 5 *E–H*; its spectral weight remains ∼100% from $Bi_2Se_3$ independent of interfacial spacing. This is consistent with the ARPES experiment observing two Dirac cones at about these two energies (Fig. 1 *G* and *H*).

From the dependence of the spectral functions on the interfacial distance in Figs. 4 and 5, we find that the original bulk $Bi_2Te_3$ Dirac cone and the newly induced Bi Dirac cone coincidentally lie

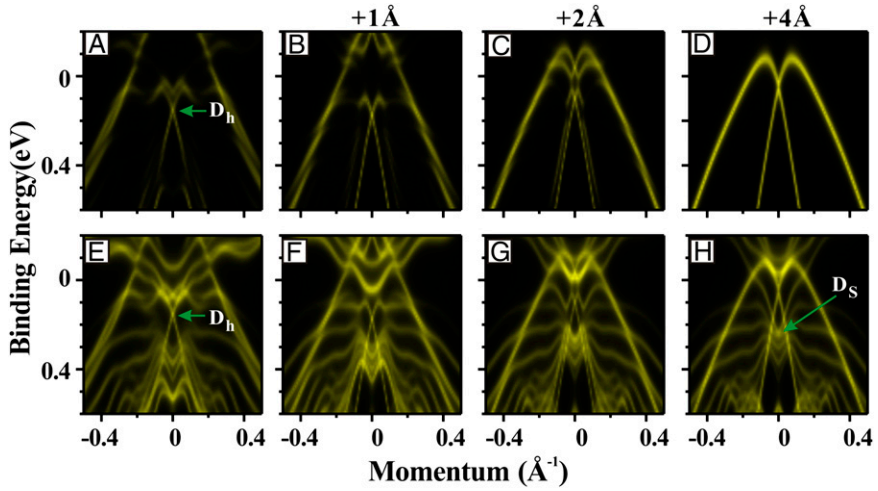


**Fig. 4.** Model theoretical energy bands as a function of interfacial distance for Bi/$Bi_2Te_3$ along M–Γ–M. (*A–D*) Contributions from top Bi bilayer and (*E–H*) contributions from top Bi bilayer plus upper 2 QL $Bi_2Te_3$. At the equilibrium position *E*, the Bi bilayer has ∼50% spectral weight at the hybrid Dirac point ($D_h$).

together at close energy proximity (both at ∼0.2 eV below the Fermi level). Because the states around the two Dirac cones are all of the surface states (2D states, Fig. 2), we suggest that the energy resonance between them leads to the enhanced many-body electronic interactions that reconstruct the spectral function into nondispersive quasiparticle features (Fig. 3*I*). In contrast, Bi/$Bi_2Se_3$ will not have this effect. We believe that the different energy position of the substrate-induced Bi Dirac cone in Bi/$Bi_2Te_3$ versus Bi/$Bi_2Se_3$ is related to both strain and interface effect. The strain effect is clearly reflected in the drastic different band structures of freestanding Bi bilayer at the respective $Bi_2Te_3$ and $Bi_2Se_3$ lattice constant, as shown in Figs. 4*D* and 5*D*. In addition, with the decreasing interfacial distance between the Bi bilayer and substrate, the interface interaction splits the Bi band and further modifies the energy position of the Bi Dirac cone.

The exact origin and nature of the many-body interaction that reconstructs the linear Dirac cone spectrum is not fully clear. However, we have performed some controlled experiments to rule out the electron–phonon interaction. By controlling the growth condition (28), we can tune the Fermi level of the $Bi_2Te_3$ substrate. The Fermi level in Fig. 1*B* is about 50 meV higher than that in Fig. 2*A*, which also moves the position of the Dirac point. On the other hand, the phonon frequency of two samples should be in the same range. If the electron–phonon coupling were significant, we would expect a change in the quasiparticle Dirac spectra because the relative energy between electron and phonon is different in the two cases. On the contrary, from the measured ARPES spectra (Fig. 1*B* versus Fig. 2*A*), we did not observe any noticeable change in the quasiparticle spectra. We have also done temperature-dependent experiments at 100 and 10 K, which additionally showed no change of quasiparticle spectra with temperature. These experimental results suggest that the electron–phonon interaction (29) is unlikely the origin.

Therefore, we think the observed quasiparticle spectra have an electronic origin. The absence of band renormalization in Bi/$Bi_2Se_3$ supports the view that the electronic many-body interaction in Bi/$Bi_2Te_3$ is associated with the hybridization of TI states, based on our comparative DFT calculations between the two systems. Another significant difference between the two systems is strain, which may play an important role in affecting the degree of many-body interaction. However, the exact form of the many-body interaction remains unclear and deserves further investigation. It

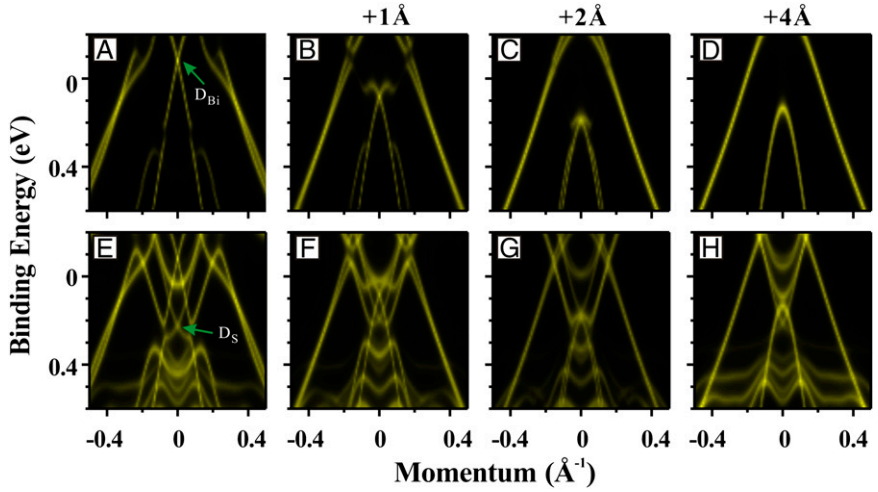


**Fig. 5.** Model theoretical energy bands as a function of interfacial distance for Bi/$Bi_2Se_3$ along M–Γ–M. (*A–D*) Contributions from top Bi bilayer and (*E–H*) contributions from top Bi bilayer plus upper 2 QL $Bi_2Se_3$. At the equilibrium position *E*, the Bi bilayer has ∼90% spectra weight at the Dirac point ($D_{Bi}$) and the 6 QL $Bi_2Se_3$ has ∼100% spectral weight at the Dirac point ($D_S$).

can be either the Coulombic electron–electron interaction or electron–plasmon interaction. For the electron–plasmon interaction, it usually shows up with satellite diamond-shaped plasmaron bands between the two Dirac points, as observed in graphene (4, 6). So far, we have not observed the diamond spectral shape but instead a vertical nondispersive feature with comparable energy and momentum resolution as refs. 4 and 6. However, the effects of disorder, sample quality, and ARPES resolution may have prevented us from observing the plasmaron bands.

## Materials and Methods

**Experimental Method.** $Bi_2Te_3$ and $Bi_2Se_3$ thin films and bulk single crystals with different Fermi energy are used as substrates. $Bi_2Se_3$ films up to 40 QLs are grown by molecular beam epitaxy method on Si (111) wafer. Bulk single crystals are grown by modified Bridgman method. Single crystals were cleaved in situ at 10 K, resulting in shiny, flat, and well-ordered surfaces. Bi films were grown on TI substrates in situ at 200 K. The thickness of Bi films was monitored by RHEED and STM. The sample temperature was kept at 100 K and/or 10 K during measurement. ARPES measurements were performed with in-laboratory He discharge lamp (He-I 21.2 eV), 28–90 eV photons at Advanced Light Source beamlines 12.0.1 and ARPES beamline in National Synchrotron Radiation Laboratory, Hefei using Scienta R4000 analyzers with base pressures better than $5 \times 10^{-11}$ torr. Energy resolution is better than 15 meV and angular resolution is better than 0.02 $Å^{-1}$.

**Computational Method.** DFT calculations for Bi(111) bilayer on $Bi_2Te_3$ and $Bi_2Se_3$ are carried out in the framework of the Perdew–Burke–Ernzerhof-type generalized gradient approximation using the VASP 4.6.31 (2007) package (30). The lattice parameters of the substrate were taken from experiments ($a$ =4.386 Å for $Bi_2Te_3$ and $a$ =4.138 Å for $Bi_2Se_3$), and the Bi bilayer is strained to match the substrate lattice parameter. All calculations are performed with a plane-wave cutoff of 600 eV on an $11 \times 11 \times 1$ Monkhorst–Pack k-point mesh. The substrate is modeled by a slab of 6 QL $Bi_2Te_3$ and $Bi_2Se_3$, and the vacuum layers are over 20 Å thick to ensure decoupling between neighboring slabs. During structural relaxation, atoms in the lower 4 QL substrate are fixed in their respective bulk positions, and the Bi bilayer and upper 2 QL of substrate are allowed to relax until the forces are smaller than 0.01 eV/Å.

**ACKNOWLEDGMENTS.** The experimental work conducted at Shanghai Jiaotong University is supported by National Basic Research Program of China Grants 2012CB927401, 2011CB921902, and 2011CB922200; National Natural Science Foundation of China Grants 91021002, 10904090, 11174199, 11134008, and 11274228; and Shanghai Committee of Science and Technology, China Grants 09JC1407500, 10QA1403300, 10JC1407100, 10PJ1405700, and 12JC1405300. The theoretical work conducted at University of Utah is supported by the office of Basic Energy Sciences, US Department of Energy Grant DE-FG02-04ER46148. D.Q. acknowledges additional support from the "ShuGuang" project supported by Shanghai Municipal Education Commission and Shanghai Education Development Foundation and from Program for Professor of Special Appointment (Eastern Scholar) at Shanghai Institutions of Higher Learning. Z.F.W. acknowledges additional support from Army Research Laboratory Cooperative Agreement W911NF-12-2-0023. W.M. acknowledges additional support from National Science Foundation-Materials Research Science and Engineering Centers Grant DMR-1121252. The Advanced Light Source is supported by the Director, Office of Science, Office of Basic Energy Sciences, of the US Department of Energy under Contract DE-AC02-05CH11231.

1. Bostwick A, Ohta T, Seyller T, Horn K, Rotenberg E (2007) Quasiparticle dynamics in graphene. *Nat Phys* 3(1):36–40.
2. Polini M, et al. (2008) Plasmons and the spectral function of graphene. *Phys Rev B* 77(8):081411.
3. Hwang EH, Sarma SD (2008) Quasiparticle spectral function in doped graphene: Electron-electron interaction effects in ARPES. *Phys Rev B* 77(8):081412.
4. Bostwick A, et al. (2010) Observation of plasmarons in quasi-freestanding doped graphene. *Science* 328(5981):999–1002.
5. Siegel DA, et al. (2011) Many-body interactions in quasi-freestanding graphene. *Proc Natl Acad Sci USA* 108(28):11365–11369.
6. Walter A, et al. (2011) Effective screening and the plasmaron bands in graphene. *Phys Rev B* 84(8):085410.
7. Kane CL, Mele EJ (2005) Quantum spin Hall effect in graphene. *Phys Rev Lett* 95(22): 226801.
8. Bernevig BA, Zhang SC (2006) Quantum spin Hall effect. *Phys Rev Lett* 96(10):106802.
9. Bernevig BA, Hughes TL, Zhang SC (2006) Quantum spin Hall effect and topological phase transition in HgTe quantum wells. *Science* 314(5806):1757–1761.
10. Fu L, Kane CL (2007) Topological insulators with inversion symmetry. *Phys Rev B* 76(4): 045302.
11. Hsieh D, et al. (2008) A topological Dirac insulator in a quantum spin Hall phase. *Nature* 452(7190):970–974.
12. Xia Y, et al. (2009) Observation of a large-gap topological-insulator class with a single Dirac cone on the surface. *Nat Phys* 5(6):398–402.
13. Zhang HJ, et al. (2009) Topological insulators in $Bi_2Se_3$, $Bi_2Te_3$ and $Sb_2Te_3$ with a single Dirac cone on the surface. *Nat Phys* 5(6):438–442.
14. Chen YL, et al. (2009) Experimental realization of a three-dimensional topological insulator, $Bi_2Te_3$. *Science* 325(5937):178–181.
15. Moore JE (2009) Topological insulators: The next generation. *Nat Phys* 5(6):378–380.
16. Hasan MZ, Kane CL (2010) Topological insulators. *Rev Mod Phys* 82(4):3045–3067.
17. Qi XL, Zhang SC (2010) The quantum spin Hall effect and topological insulators. *Phys Today* 63(1):33–38.
18. Brüne C, et al. (2011) Quantum Hall effect from the topological surface states of strained bulk HgTe. *Phys Rev Lett* 106(12):126803.
19. Kotov VN, Uchoa B, Pereira VM, Guinea F, Castro Neto AH (2012) Electron-electron interactions in graphene: Current status and perspectives. *Rev Mod Phys* 84(3):1067.
20. Das Sarma S, Hwang EH, Tse WK (2007) Many-body interaction effects in doped and undoped graphene: Fermi liquid versus non-Fermi liquid. *Phys Rev B* 75(12):121406.
21. Polini M, Asgari R, Barlas Y, Pereg-Barnea T, MacDonald AH (2007) Graphene: A pseudochiral Fermi liquid. *Solid State Commun* 143(1):58–62.
22. Hirahara T, et al. (2011) Interfacing 2D and 3D topological insulators: Bi(111) bilayer on $Bi_2Te_3$. *Phys Rev Lett* 107(16):166801.
23. Damascelli A, Hussain Z, Shen ZX (2003) Angle-resolved photoemission studies of the cuprate superconductors. *Rev Mod Phys* 73(3):473–541.
24. Liu Z, et al. (2011) Stable nontrivial Z2 topology in ultrathin Bi (111) films: A first-principles study. *Phys Rev Lett* 107(13):136805.
25. Murakami S (2006) Quantum spin Hall effect and enhanced magnetic response by spin-orbit coupling. *Phys Rev Lett* 97(23):236805.
26. Wada M, Murakami S, Freimuth F, Bihlmayer G (2011) Localized edge states in two-dimensional topological insulators: Ultrathin Bi films. *Phys Rev B* 83(12):121310.
27. Koroteev YM, Gihlmayer G, Chulkov EV, Blugel S (2008) First-principles investigation of structural and electronic properties of ultrathin Bi films. *Phys Rev B Condens Matter* 77(4):045428.
28. Wang G, et al. (2011) Topological insulator thin films of $Bi_2Te_3$ with controlled electronic structure. *Adv Mater (Deerfield Beach Fla)* 23(26):2929–2932.
29. Hatch RC, et al. (2011) Stability of the $Bi_2Se_3$(111) topological state: Electron-phonon and electron-defect scattering. *Phys Rev B* 83(24):241303.
30. Kresse G, Hafner J (1993) *Ab initio* molecular dynamics for liquid metals. *Phys Rev B Condens Matter* 47(1):558–561.